Molecular Simulations of Dodecyl-D-Maltoside Micelles in Water: Influence of the Headgroup Conformation and the Force Field Parameters

ARTICLE *in* THE JOURNAL OF PHYSICAL CHEMISTRY B · JANUARY 2011

Impact Factor: 3.3 · DOI: 10.1021/jp109545v · Source: PubMed

Molecular Simulations of Dodecyl-β-maltoside Micelles in Water: Influence of the Headgroup Conformation and Force Field Parameters

Stéphane Abel,*,† François-Yves Dupradeau,‡ E. Prabhu Raman,§ Alexander D. MacKerell, Jr.,§ and Massimo Marchi†

Commissariat à l'Energie Atomique, DSV/iBiTEC-S/SB²SM/LBMS & CNRS URA 2096, Centre d'Etudes, Saclay, F-91191 Gif-sur-Yvette Cedex, France, CNRS URA2096, F-91191, Gif-sur-Yvette Cedex, France, Laboratoire des glucides, UFR de Pharmacie & CNRS UMR 6219, Université de Picardie - Jules Verne, Amiens, France, and Department of Pharmaceutical Sciences, School of Pharmacy, University of Maryland, Baltimore, Maryland, United States

Received: October 5, 2010; Revised Manuscript Received: November 21, 2010

This paper deals with the development and validation of new potential parameter sets, based on the CHARMM36 and GLYCAM06 force fields, to simulate micelles of the two anomeric forms (α and β) of *N*-dodecyl-β-maltoside ($C_{12}G_2$), a surfactant widely used in the extraction and purification of membrane proteins. In this context, properties such as size, shape, internal structure, and hydration of the $C_{12}G_2$ anomer micelles were thoroughly investigated by molecular dynamics simulations and the results compared with experiments. Additional simulations were also performed with the older CHARMM22 force field for carbohydrates (Kuttel, M.; et al. *J. Comput. Chem.* **2002**, *23*, 1236−1243). We find that our CHARMM and GLYCAM parameter sets yield similar results in the case of properties related to the micelle structure but differ for other properties such as the headgroup conformation or the micelle hydration. In agreement with experiments, our results show that for all model potentials the β-$C_{12}G_2$ micelles have a more pronounced ellipsoidal shape than those containing α anomers. The computed radius of gyration is 20.2 and 25.4 Å for the α- and β-anomer micelles, respectively. Finally, we show that depending on the potential the water translational diffusion of the interfacial water is 7−11.5 times slower than that of bulk water due to the entrapment of the water in the micelle crevices. This retardation is independent of the headgroup in α- or β-anomers.

I. Introduction

Glycolipids (GLs) are glycosyl derivatives of lipids that belong to a large family of molecules known as glycoconjugates.[1] From a chemical point of view, GLs designate any molecule with surfactant properties containing a carbohydrate headgroup (with one or more monosaccharide units) attached to a lipophilic tail. In particular, alkyl-glycosides are simple glycolipid molecules obtained, for instance, by condensation such as "Fischer glycosidation" of a sugar with a fatty alcohol.[2] Their tension-active properties depend on the length of the alkyl chain.[3,4] Because they are highly effective, ecologic, and nontoxic, this class of surfactants has a wide range of applications in food, cosmetic, and pharmaceutical industries.[5−7] Similar to other surfactants, GLs can form different mesophases in water, such as micelles, lamellae, vesicles, etc., depending on the experimental conditions (see, for instance, refs 3 and 8−15).

During the last decades, alkyl-glucosides have also attracted a great deal of interest in the context of membrane protein extraction[16,17] given that they have a low critical micellar concentration (cmc) around 10^{-3}−10^{-4} mol·L^{-1} (see Table 2 of ref 7 for data and references), form large aggregates, and keep the protein structure and its activity intact.[18,19] In particular, alkyl-glucosides have been successfully used for solubilization of large membrane protein complexes, such as rhodopsin,[20] cytochrome c oxidase,[21,22] and protein channel.[23,24]

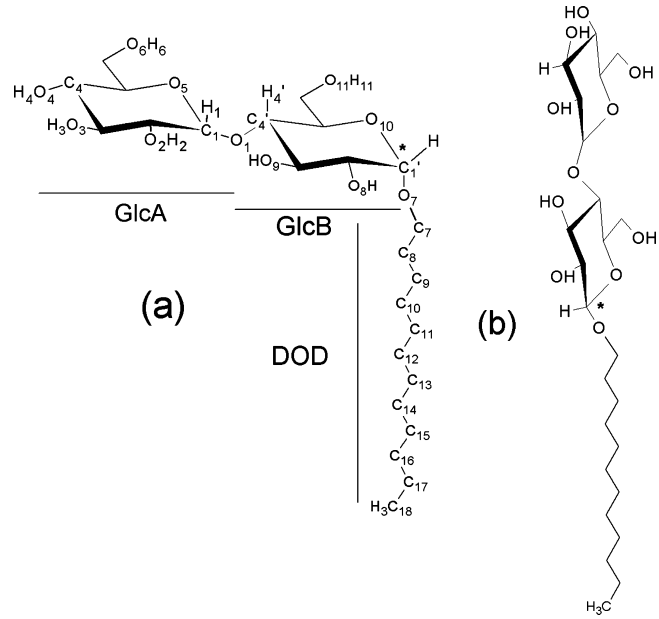

Figure 1. The α- (a) and β-anomers (b) of $C_{12}G_2$ surfactants with the atom numbering scheme used in the paper. The anomeric center C_1' of the molecule is underlined with a star.

Among these detergents, *N*-dodecyl-β-maltoside ($C_{12}G_2$) (Figure 1) is one of the most used alkyl-glucosides in membrane protein extraction experiments.[17] Two anomers, α- and β-, exist for $C_{12}G_2$ due to two possible connectivities of the dodecane chain (DOD) and of the anomeric carbon (C_1') linking DOD to

* Corresponding author. E-mail: stephane.abel@cea.fr.
† DSV/iBiTEC-S/SB2SM/LBMS & CNRS URA2096.
‡ Université de Picardie - Jules Verne.
§ University of Maryland.

10.1021/jp109545v

the maltose head. The β-isomer is in a linear conformation, whereas the α-isomer is in a right-angle bent formed between the maltose headgroup and the alkyl tail. The α-anomer is less soluble than the β-anomer[7,25] and is not commonly used in membrane protein studies, albeit with some notable exceptions. For instance, in the bacterial *E. coli* Na^+/H^+ antiporter, it was reported recently[24] that the α-$C_{12}G_2$ surfactant is needed to obtain a crystallized protein in its native state. To explain this feature, it is generally assumed that the orientation of the maltose head in the surfactant leads to differences in sterical constraints (i.e., due to different packing parameters) and, possibly, in hydration behaviors. SANS and SAXS scattering experiments have shown that the α-anomer of $C_{12}G_2$ forms a small quasi-spherical micelle, while the β-conformation forms large oblate aggregates.[13,26]

In the past few years, molecular dynamics simulations (MD) have been extensively used to study the structure and hydration of mono- and disaccharides, in aqueous solutions (e.g., refs 27−40). MD with alkyl-glycosides (such as alkyl-β-*O*-glucoside (C_8Glc_1) or alkyl-β-*O*-galactoside (C_8Gal)) have also been performed in the past, involving bilayers[41−43] or micelles[44−47] or interacting with a plant protein.[48] In the studies of Bogusz et al.[44] and Chong et al.,[47] the influence of the surfactant headgroup conformation on the micelle structure and hydration has been thoroughly examined. It was reported that despite the conformational changes in the headgroup, several properties remain nearly unchanged for the aggregates, in particular micelle shape, surfactant tail length, and conformation. In contrast, other properties directly related to the interaction between the solvent and the headgroup (i.e., solvent accessible surface area, headgroup cluster structure, number of isolated water molecules at the micelle surface) are significantly modified by the stereochemistry of the carbohydrate head.[44,47] It was also noted that the sugar counterpart is responsible for strong perturbations of the water structure at the micelle surface and it affects the formation of a large hydrogen bond (HB) network at the micelle surface between water and the headgroups, and within the headgroups themselves (inter- and intra-HBs, respectively).[41,47,49] This HB network may also explain the good thermal stability of the surfactants[49] and cryoprotective effects.[36,50]

Despite their crucial role in membrane protein extractions, $C_{12}G_2$ micelles have rarely been studied by computational methods, and to our knowledge, only a single MD study has been performed on these systems in the past.[51] That investigation was mainly focused on the hydration properties of the micelles and used a thermodynamical approach to examine the micellization behavior of surfactants with different chemical nature, and was compared with experiments. To simplify the calculations, the simulations were carried out starting from a spherical aggregate of 45 β-$C_{12}G_2$. This aggregation number is far from that of 130, commonly accepted in the literature.[13,14,26] Moreover, the authors used the OPLS-AA force field not fully optimized for glycolipid molecules.[52] In absence of optimized parameters for the two $C_{12}G_2$ anomers for the widely used CHARMM and GLYCAM06 force fields, we have developed two sets of parameters compatible with these force fields for condensed-phase MD simulation studies. We expect that these new parameters will allow us to examine the influence of the headgroup stereochemistry in $C_{12}G_2$ micelle structures under experimental conditions. Our endeavor included the calculations of new RESP atomic charges for the current GLYCAM06 potential and an optimization of the dihedral angles for the acetal linkage between the maltose headgroup and the alkyl chain for both of the α- and β-anomers compatible with the CHARMM36 force field (see next sections). These new CHARMM and GLYCAM parameters (named GLYCAM06 and CHARMM-Opt, respectively) have been tested and validated by performing different MD simulations of two realistic models of $C_{12}G_2$ micelles in explicit water. To compare our results with previous MD studies of glycolipid micelles,[44−46] we have also performed two simulations with the old CHARMM22 parameters taken from Kuttel et al.[53] and Reiling et al.,[54] named throughout the paper with the acronym CHARMM-K.

This paper is organized as follows: in the next sections, we describe the procedures followed to derive RESP atomic charges as well as the optimization of the dihedral angles for the acetal linkage for the α- and β-anomers for the GLYCAM and CHARMM force fields. This is followed by sections covering MD simulations, the results, as well as the interpretations of these results.

II. Methods

1. RESP Charge Derivation for the α- and β-Anomers of $C_{12}G_2$ for GLYCAM. RESP charge derivation for $C_{12}G_2$ GL for the GLYCAM force field was carried out using standard methods.[55−57] For this purpose, we have followed a similar approach to that described by Gouin et al.[39] Three molecules, i.e., methyl α-*D*-glucopyranoside (AMG), methyl β-*D*-glucopyranoside (BMG), and 1-dodecanol (OH-DOD), were involved in charge derivation. For each glucose unit, two rotamers were selected for the ω (i.e., represented by the $O_6C_6C_5C_4$ and $O_6C_6C_5O_5$ rotational angles) in the *gauche*−*gauche* (*gg*, $\omega = -60°$) and *gauche*−*trans* (*gt*, $\omega = +60°$) conformations (see Figure S1 in the Supporting Information) considering that they are the most populated in solution.[58] Optimized geometries presenting intramolecular HBs were excluded from charge derivation to avoid the overpolarization effect.[56] As a consequence, geometry optimization was carried out with dihedral angle constraints. The $HO_4'O_4'C_4H_4'$ dihedral angle of the glucosides AMG and BMG was constrained to 180°, whereas the $HO_3-O_3-C_3-H_3$ and $HO_2-O_2-C_2-H_2$ dihedrals of AMG and BMG were constrained to 180°, respectively. A single conformation for 1-dodecanol was considered in charge derivation, and the selected geometry was optimized in its extended conformation (i.e., "all-*trans* dihedrals"). Indeed, it has been previously shown that the surfactant alkyl chain adopts mainly this conformation in the micelle core (see, for instance, refs 44, 59, and 60). Frequencies were calculated for all the molecules, and transition state structures were excluded from the charge derivation procedure. Geometry optimization, frequency calculation, and molecular electrostatic potential (MEP) computation were carried out using the Gaussian 03 quantum mechanics (QM) package in the gas phase,[61] whereas charge fitting was performed using the RESP program.[55,56] The HF/6-31G** level of theory was used in the geometry optimization and frequency calculations,[62] while MEP computation was based on HF/6-31G*, leading to implicit polarization required in condensed phase simulations when using the nonadditive AMBER force field model.[55,56] The CHELPG algorithm was used to compute the grid of points involved in MEP computation.[63] The molecular orientation of each optimized geometry was controlled using the rigid-body reorientation algorithm implemented in the RED program.[63] Four molecular orientations for each optimized geometry of AMG and BMG (based on the glucose atom names $C_1C_3C_5$, $C_5C_3C_1$, $C_2C_4O_5$, and $O_5C_4C_2$; see Figure S1 in the Supporting Information) and for the alkyl chain (based on the 1-dodecanol atom names $C_1C_2C_3$, $C_3C_2C_1$, $C_1C_3C_5$, and $C_5C_3C_1$; see Figure S1 in the Supporting Information) were generated before MEP computation, and involved in the charge

fitting procedure to yield reproducible atomic charges. Charge fitting was performed using a single RESP stage with a hyperbolic constraint value of 0.01. Intramolecular charge constraints between the methyl and the C4 hydroxyl groups of AMG and BMG and intermolecular charge constraints between the methyl group of each methyl glucoside and the hydroxyl group of OH-DOD (Figure S1, Supporting Information) were set to a value of zero during charge fitting, allowing the definition of the molecular fragments and force field libraries required to build $C_{12}G_2$ GL. Each hydrogen atom bound to an sp3 carbon was also constrained to a target value of zero during charge fitting to ensure a compatibility with the GLYCAM force field.[64] The charge derivation procedure was automatically carried out using version IV of the R.E.D. program.[63] RESP charges for the α- and β-anomers of $C_{12}G_2$ are reported in the Supporting Information, and are freely available from the R.E.D.D.B. server (http://q4md-forcefieldtools.org/REDDB/)[65] with the accession code "F-72".

2. Optimization of the Dihedral Angle Potentials for the Acetal Linkage in α- and β-$C_{12}G_2$ for CHARMM. Ethoxy tetrahydropyran (Et-THP) was used as a model compound to parametrize the acetal linkage in $C_{12}G_2$ GL. α- and β-Substituted anomers were involved in the study (Figure S2, Supporting Information). Tetrahydropyran (THP) parameters were those previously developed in the context of hexopyranoses.[66] The bond, angle, dihedral, Lennard-Jones, and partial charge parameters involving the acetal group were transferred by analogy to methoxy-THP (Met-THP) parameters developed previously[67] and existing linear ether parameters (Listing S1, Supporting Information).[68] The optimization of these transferred parameters was undertaken as follows. QM MP2/cc-pVTZ//MP2/6-31G* Φ/Ψ scans for both α- and β-anomers were performed ($\Phi = O_R-C_1-O_E-C_6$, $\Psi = C_1-O_E-C_6-C_7$) at 15° increments, thus giving rise to 576 conformations as target data. Figure S3 in the Supporting Information shows that the transferred parameters serve as a good initial guess, as they reproduce the QM energy surface satisfactorily. The dihedral parameters involving the exocyclic heavy atoms were directly fitted using the MCSA automated dihedral fitting procedure[69] to the QM Φ/Ψ data, resulting in a marked improvement in the root-mean-square error (RMSE) from 2.01 (1.23) to 0.81 (0.83) kcal/mol for both the α- and β-anomer. Figure S3 in the Supporting Information shows that the fit parameters reproduce well the QM Φ/Ψ potential energy surface for both anomers. Additionally, Figure S4 in the Supporting Information shows that the fitted parameters reproduce the 1-D QM energy as a function of Ψ (Φ is kept constant at ±60° for the α- and β-anomer) much better than the transferred ones. Unconstrained MP2/6-31G* optimization of the molecules revealed the QM global minima for the α-anomer at values (61.5°, 175.1°) and for the β-anomer at values of (−63.2°, −172°). These QM minima are correctly reproduced by our optimized dihedral parameters, as seen in Table S2 in the Supporting Information. We also notice that they also well reproduce the energy difference between the global minima of the two anomers, $\Delta E_{\alpha-\beta}$ ($\Delta E_{\alpha-\beta} = -1.52$ kcal/mol for QM and $\Delta E_{\alpha-\beta} = -1.85$ kcal/mol for MM).

The transferred partial charge on the ether oxygen atom (O_E) was validated by performing water pair interaction energy calculations as performed in previous studies.[66] This consists of optimizing the solute/water interaction distance at the HF/6-31G* level of theory, with constraints on all other degrees of freedom. Table S3 in the Supporting Information shows that our parameters reproduce well the scaled QM interaction energies and adjusted distances,[66] thus validating the transfer of charges. These new sets of parameters are provided in the Supporting Information in the CHARMM readable format (Listing S1, Supporting Information).

3. Simulation Methods. To be consistent with the force fields developed in this study, we used an "all-atom" approach to model all micellar systems. RESP charges derived in section II.1 were involved in GLYCAM-based MD simulations with the bonded and nonbonded parameters taken from the GLYCAM06 force field version *f*.[64] The 1−4 van der Waals and electrostatic scaling factors were set to 1.0, in agreement with the developer recommendations.[64] In the case of the CHARMM-K simulations, we used two sets of parameters to model the sugar headgroup and the exocyclic atom connecting the maltose head and the alkyl chain. For the maltose head, we used the parameters of Kuttel et al.[53] (a revision of the CHARMM22 force field for sugars of Ha et al.)[70] and for the acetal atom those of Reiling et al.,[54] which is assigned to an ether oxygen atom type with a partial charge of −0.30 e. These two sets of parameters were previously employed by Bogusz et al.[44,45] and Konidala et al.[46] in MD simulations of C_8G_1 micelles in water. For the CHARMM-Opt simulations, we used the new set of parameters for hexopyranose[66] with optimized parameters for the Φ_H/Ψ_H glycosidic dihedral angles which significantly improves the CHARMM force field for simulations of polysaccharides.[67] For the connection between the maltose head and the alkyl chain, we adopted the optimized parameter set for ethers by Lee et al.[71] combined with the optimized torsion parameters developed for Et-THP described in the previous section II.2. For all MDs performed with the CHARMM force fields, the alkyl chain of the surfactant was modeled with parameters developed by Klauda et al. for alkanes.[72] This contrasts with previous investigations[44,45] and the work of Konidala et al.[46] where for alkyl chain the dihedral parameters described in ref 73 were used. Finally, the TIP3P water model[73] was adopted to model the solvent for all the simulations.

4. Construction of the Micelles and Simulation Techniques. In this paper, we made the choice of using two *preassembled* micelles with 75 and 132 monomers of α- and β-$C_{12}G_2$, respectively. For the three different force fields studied in this work, the same approach was used to construct the six micelles and an identical protocol was applied in MD simulations. The aggregation numbers (N_{det}) were obtained by Dupuy et al.[13] by fitting the scattering curves from SAXS and SANS experiments at a temperature of 297 K and a concentration range between 20 and 100 mM for monodispersed micelles. We should emphasize that the N_{det} values may depend on the experimental methods and on the concentration. For example, the N_{det} value for the β-$C_{12}G_2$ micelle used here is higher than the value of 98 found by Rosevear et al.[74] using the gel filtration method, the value of 82−120 obtained by SAXS measurements[26] at 310 K, and the value of 111 ± 10 derived by time resolved fluorescence quenching (TRFQ) spectroscopy.[75] On the other hand, our N_{det} value is well within the findings of other experiments, e.g., $N_{det} = 125 \pm 10$ was reported using other TRFQ results at 4.89−19.6 mM and 289−333 K,[14] whereas $N_{det} = 135-145$ was found by Lipfert et al.[76] by SAXS at 298 K. In the case of the α-$C_{12}G_2$ micelle, only one aggregation number has been reported in the literature, $N_{det} = 75$.[13]

The initial configurations of the two aggregates were constructed using the Packmol program.[77] This program created initial condition for MD by packing in the sphere N_{det} $C_{12}G_2$ molecules in their extended conformation, with the first carbon atom (C_7) of the alkyl chain, near the headgroup at ∼17 Å from the center of the micelle. This is larger than the total length

TABLE 1: Parameters for Micelle Simulations[a]

system	α-$C_{12}G_2$	β-$C_{12}G_2$
$N_{C_{12}G_2}$	75	132
N_{H_2O}	13771	18389
N_{atm}	47388	65859
$m_{C_{12}G_2}/m_{Tot}$	13.4	16.9
T (K)	297	297
t_{sim} (ns)	14.0	14.0
ρ (g/cm^3)	1.02 ± 0.01	1.03 ± 0.01

[a] $N_{C_{12}G_2}$, N_{H_2O}, and N_{atm} are the numbers of *N*-dodecyl-β-*D*-maltopyranoside monomers ($C_{12}G_2$), water, and atoms composing the simulated systems. $m_{C_{12}G_2}/m_{Tot}$ is the weight concentration (in %) of $C_{12}G_2$ in each system. t_{sim} is the simulation time (the 300 ps equilibration period was excluded from the analysis).

(∼14.0 Å) of the DOD chain in an extended conformation obtained with the DS Visualizer v2.0 (Accelrys Inc., San Diego, CA) modeling program. In this way, the number of "steric clashes" for the terminal ethyl groups of the $C_{12}G_2$ alkyl chain is reduced. To remove other inter- and intramolecular overlaps, additional stages of conjugate gradient minimization followed by MD equilibration in a vacuum with a small time step were carried out. Following this step, the headgroups were randomized by running MD simulations of the aggregates at 450 K for 300 ps, with the surfactant tails kept fixed to their minimized conformation. From this point on, in all cases, the systems were solvated by adding TIP3P water at standard density in a truncated octahedron cell, corresponding to a simple cubic primitive cell unit with parameters $a = b = c$ and $\alpha = \beta = \gamma = 109.472°$. Given the two different N_{det} values used in our study, we chose $a = 85$ Å and $a = 95$ Å for the simulations of the α- and β-anomers, respectively. These box sizes were chosen to ensure that all the molecular systems were within the experimental L_1 phase (i.e, <45 % in weight concentration),[75] and that there was a sufficient distance (∼15 Å) between the micelle surface and the edge of the box to minimize interactions with periodic images.[78] As shown in Table 1, where we provide the composition of the two simulated systems, the simulated concentrations of the detergent are near 0.3 and 0.40 M for the α- and β-$C_{12}G_2$ anomers, respectively. This is higher than the surfactant concentration used in the experimental study of Dupuy et al.[13] (0.02−0.04 mol·L^{-1}) and higher than the critical micelle concentration (cmc) for the α- and β-$C_{12}G_2$ (∼1.5×10^{-4} and ∼2.0×10^{-4} mol·L^{-1}, respectively)[13,75] at a temperature of 298 K. Indeed, simulations near the cmc would require about 2000 times more water in the simulation system, leading to a dramatic increase of the calculation time. Furthermore, in order to equilibrate the solvent molecules, the systems were run for 300 ps at 450 K, with the ensemble of the micelle atoms fixed to their initial positions. Then, the constrained micelle atoms were released and the system slowly heated from 0 to 297 K in 300 ps as described in ref 79. Finally, the resulting conformations were simulated in the NPT ensemble ($T = 297$ K and $P = 0.1$ MPa) for 14 ns after discarding the initial 300 ps. MD snapshots were saved every 240 fs for subsequent analysis.

5. Molecular Dynamics. For all the simulations and analysis performed in this study, serial and parallel versions of the ORAC code were used.[80] To simulate in the NPT ensemble, ORAC uses a method based on the extended system approach by adding extra (virtual) coordinates and momenta in the system to control the temperature and the pressure.[81−85] To integrate the equation of motion, a five-time-step r-RESPA integration scheme with a Liouvillean separation in three nonbonded shells was used.[86] The procedure combines the smooth particle mesh Ewald (SPME) method to handle electrostatic interactions[87] and the method of constraints to keep the covalent bonds involving hydrogens at their equilibrium length.[88] The SPME parameters were chosen to maintain a relative error of less than 0.1% on the electrostatic interactions for all the micelles. For this purpose, a convergence parameter of $\alpha = 0.43$ Å^{-1}, a fifth-order B-spline, and a 96 grid points in each Cartesian direction to take care of the SPME charge interpolation for each simulated system was used.

III. Results

First, we consider the general structure of the α- and β-$C_{12}G_2$ aggregates at different simulation times: $t_{sim} \approx 0$ fs, $t_{sim} = 7.0$ ns, and $t_{sim} = 14.0$ ns of the production period. Figure 2 provides three snapshots for each type of $C_{12}G_2$ micelle taken from the CHARMM-Opt simulations; these results are representative of the other simulations described in this paper. Visual inspection of the figure shows that, at the beginning of the run, the micelles have rougher surfaces with some glycolipid protrusions (see Figure 2a and d). Thus, the micelles present large solvent-exposed surfaces where the alkyl chains of the surfactant are exposed to the solvent (see below). However, after typically 2−3 ns of production, Figure 2b−e, the surfactants arrange themselves to form compact aggregates where a major part of the alkyl tails are buried and the surface is covered with the glycolipid headgroups. These pictures also show that the α- and β-$C_{12}G_2$ micelles are not perfectly spherical and that the β-$C_{12}G_2$ micelle is more ellipsoidal than the α-one (see below). This finding has been observed in the different MD simulations performed in this study, regardless of the force field. Finally, in contrast with previous simulations[46,47] of octyl-β-glucoside micelles, the integrity of the micelles studied with the GLYCAM and CHARMM force fields is maintained all along our simulation time window (14 ns), and no surfactant molecules escaped from the micelle. This is consistent with previous experimental results obtained for alkyl-maltoside micelles where it was found that the monomer exchange time between the micelle and the solvent is in the order of 0.1−1.2 μs.[89]

A. Size of the Micelles. To examine the stability and to measure the dimensions of the micelle in the six runs, we have computed their instantaneous radii of gyration, R_g, over the course of the simulations (Figure 3) using the following expression:

$$R_g^2 = \sum_i m_i (r_i - r_{cm})^2 \Big/ \sum_i m_i \qquad (1)$$

where m_i is the mass of atom i of the micelle at the distance r_i from the center of mass r_{cm}. For all the micelles studied here, the R_g values are stable after typically ∼3 ns of production. As indicated previously, during the beginning of the productive run (i.e., between ∼0 and 3 ns time period), local arrangements and compaction of the surfactants on the micelle surfaces are observed. This feature was also observed in previous glycolipid micelle simulations.[47]

The instantaneous R_g values for the α-$C_{12}G_2$ micelle in the three runs stabilizes after ∼3 ns around ∼20−21 Å until the end of the trajectory. The average R_g values, $\langle R_g \rangle$, of the α-$C_{12}G_2$ micelles, computed from the last 11 ns of CHARMM-K, CHARMM-Opt, and GLYCAM06 runs (20.5 ± 0.1, 20.2 ± 0.1, and 20.0 ± 0.1 Å, respectively) are close to the R_g experimental value (18.6 ± 0.6 Å[13]) calculated from the semiaxis lengths of the micelle a_M, b_M, and c_M and the expression $R_g^2 =$

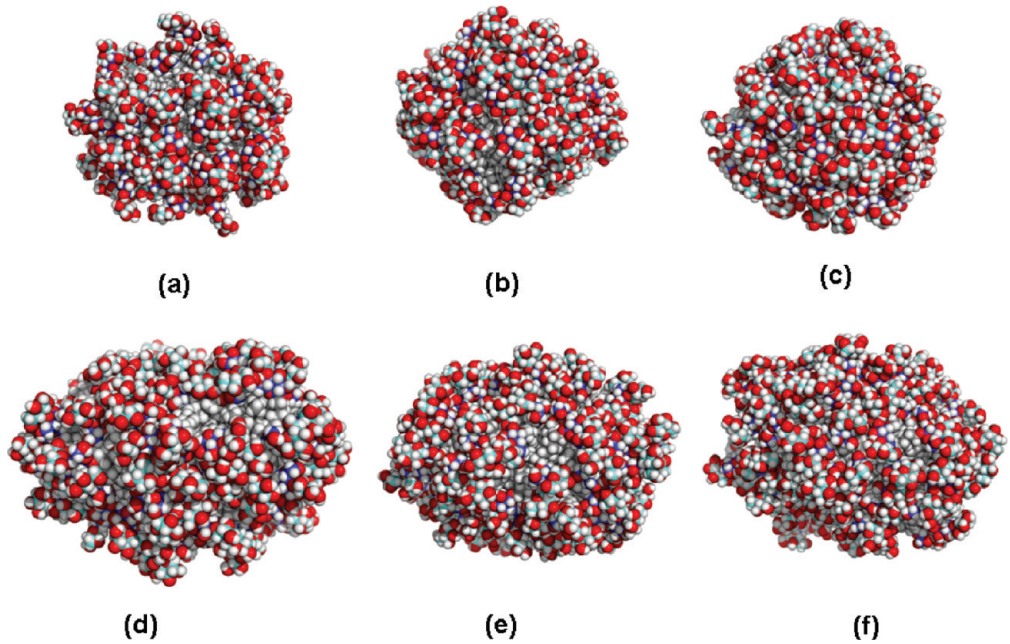

Figure 2. Representative MD snapshots of the α- (a−c) and β-anomers (d−f) of $C_{12}G_2$ micelles simulated with the CHARMM-Opt force field at $t \approx 240$ fs (a, d), $t \approx 7.0$ ns (b, e), and $t \approx 14$ ns (c, f) of the production period. Oxygen and hydrogen are in red and white. Carbons in GlcA, GlcB, and the alkyl chain are blue, cyan, and gray, respectively. Water molecules are removed for visual clarity. Graphics were produced with the PyMOL program.[122]

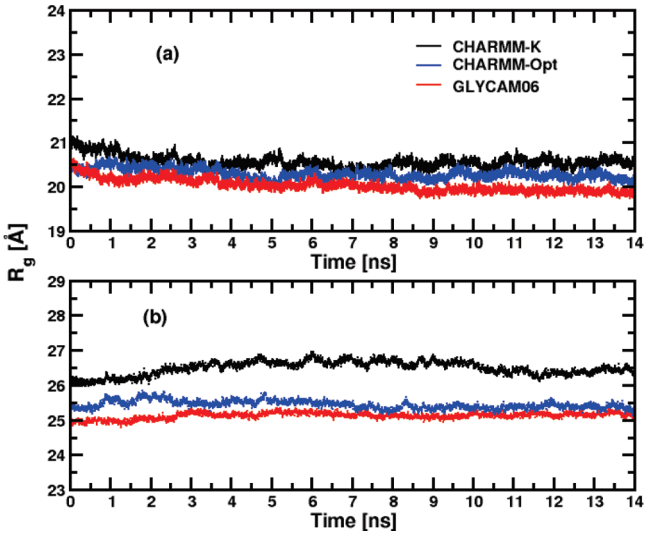

Figure 3. Time evolution of the radius of gyration, R_g, for α- (a) and β-anomers (b) of $C_{12}G_2$ micelles.

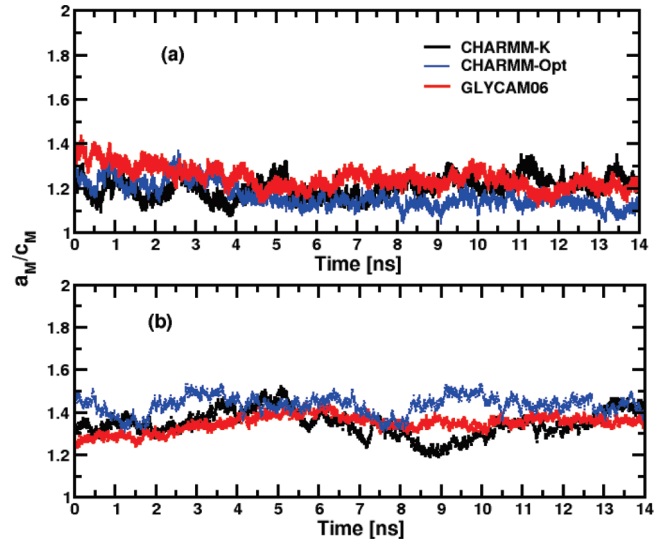

Figure 4. Time evolution of the major and minor semiaxis of inertia ratio for α- (a) and β-anomers (b) of $C_{12}G_2$ micelles.

$(a_M^2 + b_M^2 + c_M^2)/5$ for an ellipsoid with a uniform density.[79] In the case of the β-$C_{12}G_2$ micelles, R_g reached stable values after ∼2.5−3 ns depending on the force field used. In contrast to the α-$C_{12}G_2$ simulations, the three force fields lead to significant differences (up to 1.0 Å) for the instantaneous and averaged R_g, especially for the two CHARMM force field versions. For β-$C_{12}G_2$, the $\langle R_g \rangle$'s are equal to 26.4 ± 0.1, 25.4 ± 0.1, and 25.1 ± 0.1 Å, for the aggregates simulated with the CHARMM-K, CHARMM-Opt, and GLYCAM06, respectively. The $\langle R_g \rangle$'s obtained with the CHARMM-Opt and GLYCAM06 parameters are closer to the experimental value of 23.3 ± 0.6 Å.[13]

B. Shape of the Micelles. The micelle shape can be characterized by computing the instantaneous ellipsoidal axis ratio between the micelle major (a_M) and minor (c_M) semiaxis lengths, or a_M/c_M, obtained from the inertia tensors (see ref 79 for details). As shown in Figure 4, the six micelles present a stable ellipsoidal shape (i.e., $a_M/c_M > 1.0$) after typically ∼4.0 ns. For the α-$C_{12}G_2$ micelles, their shapes do not depend significantly on the force field. This contrasts with the behaviors of the β-$C_{12}G_2$ micelles where the ratio a_M/c_M shows much larger fluctuations. To be consistent with the calculation of R_g, the initial 3 ns of each trajectory were discarded in the calculation of a_M/c_M. The average values of the ratio, $\langle a_M/c_M \rangle$, are reported in the seventh column of Table 2 for the different micelles studied. In our calculation, both α- and β-$C_{12}G_2$ are ellipsoidal, but α-$C_{12}G_2$ is the closest to the shape of a sphere. In the case of β-$C_{12}G_2$ aggregates, the instantaneous a_M/c_M values stabilize around ∼1.40 at the end of the simulations independently of the considered force field and the $\langle a_M/c_M \rangle$ values are close for the three micelles: 1.38 ± 0.03, 1.43 ± 0.01, and 1.38 ± 0.04 for CHARMM-K, CHARMM-Opt, and GLYCAM06, respectively. In contrast, β-$C_{12}G_2$ micelles have a pronounced *oblate* shape ($a_M > b_M \approx c_M$), which agrees well with the experimental

TABLE 2: Average Dimensions and Shapes of the Six Micelles[a]

force field	micelle	$\langle R_g \rangle$	$\langle a_M \rangle$	$\langle b_M \rangle$	$\langle c_M \rangle$	$\langle a_M/c_M \rangle$	$\langle a_{HC} \rangle$	$\langle b_{HC} \rangle$	$\langle c_{HC} \rangle$	$\langle l_{pl} \rangle$
CHARMM-K	α-$C_{12}G_2$	20.5	28.4	25.6	23.8	1.20	22.1	19.1	16.5	6.7
	β-$C_{12}G_2$	26.4	38.8	34.7	28.1	1.38	33.1	27.3	20.0	7.2
CHARMM-Opt	α-$C_{12}G_2$	20.2	27.8	26.1	24.3	1.14	21.5	19.1	16.7	7.0
	β-$C_{12}G_2$	25.4	38.1	33.0	26.5	1.43	30.6	24.8	19.3	7.7
GLYCAM06	α-$C_{12}G_2$	20.0	28.4	25.5	23.1	1.23	22.3	18.6	16.5	6.5
	β-$C_{12}G_2$	25.2	37.2	32.0	30.1	1.38	30.1	24.4	19.2	7.2

[a] $\langle ... \rangle$ stands for the ensemble average. Values with M and HC subscripts were computed by including all the micelle atoms and those of the hydrophobic core, respectively. The radii of gyration and the semi-axis lengths were computed using the inertia tensor (e.g., see ref 79) and the main text for details. $\langle l_{pl} \rangle$ is the average polar layer thickness of the micelle in Å. The statistical errors (maximum errors) are always lower than 0.1, 0.8, and 0.3 Å for R_g, semi-axis lengths, and polar layer thickness, respectively.

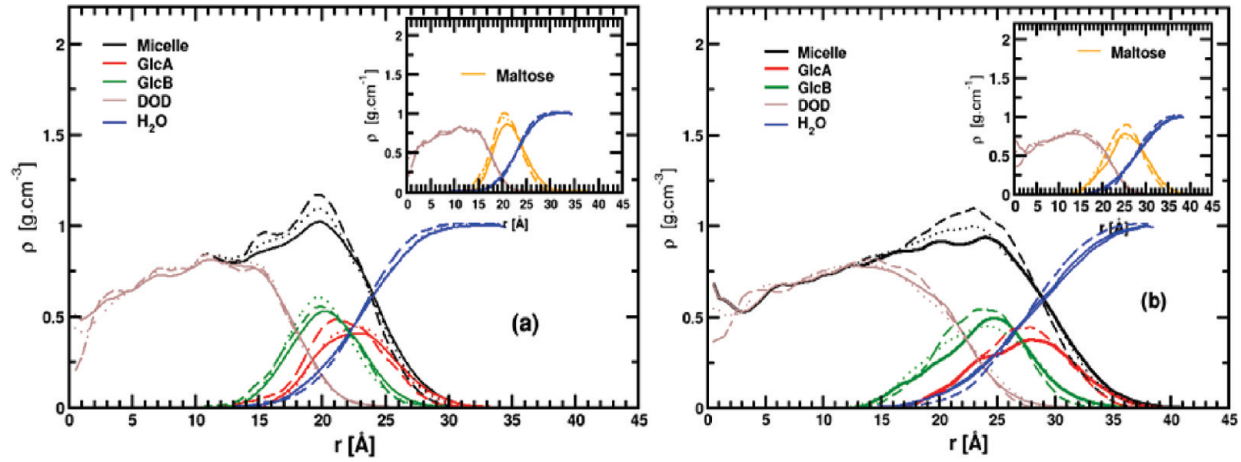

Figure 5. Average radial density profiles with respect to the center of mass ($r = 0$ Å) for simulations performed with CHARMM-K (continuous line), CHARMM-Opt (dotted lines), and GLYCAM06 force fields (dashed line) for α- (a) and β-anomers (b) of $C_{12}G_2$ micelles. In the inset, the radial profiles for the micelle hydrophobic core (maroon), the maltose headgroup (orange), and water (blue) are plotted. A 0.5 Å bin width was used for both figures.

observations.[13,26,75] However, we must emphasize that the $\langle a_M/c_M \rangle$ values for the β-$C_{12}G_2$ micelles remain, depending on the force field, lower than the estimated experimental values (i.e., $a_M/c_M = 1.70$ from Dupuy et al.).[13]

The instantaneous length values of the semiaxis of each micelle hydrophobic core (i.e., a_{HC}, b_{HC}, and c_{HC}) have also been computed by including only the contributions from the surfactant hydrophobic chain in the calculations of the inertia tensors. The average values of the three semiaxes ($\langle a_{HC} \rangle$, $\langle b_{HC} \rangle$, and $\langle c_{HC} \rangle$) are reported in the 8th, 9th, and 10th columns of Table 2. We find that the average major and minor semiaxis lengths $\langle a_{HC} \rangle$ and $\langle c_{HC} \rangle$ are in relative agreement with experimental values for α-$C_{12}G_2$ and β-$C_{12}G_2$ (i.e., $\langle a_{HC} \rangle = \langle c_{HC} \rangle = 18.6 \pm 1.0$ Å and $\langle a_{HC} \rangle = 28.2 \pm 1.0$ Å and $\langle c_{HC} \rangle = 14.1 \pm 1.0$ Å, respectively).[13] The average thickness of the polar outer layer, or $\langle l_{pl} \rangle$, computed by subtracting the semiaxis length of the hydrophobic core from those of the whole micelle ($\langle a_M \rangle$, $\langle b_M \rangle$, and $\langle c_M \rangle$) does not change significantly with the force field and is 6.7 ± 0.3 Å for the α-anomer of the $C_{12}G_2$ and increases up to 7.3 ± 0.4 Å for the β-anomer. Due to the partial folding of the maltose head, these values are 39.1 and 33.4% smaller than the calculated length of the maltose in its extended configuration (~11.0 Å). The larger $\langle l_{pl} \rangle$ value for β-$C_{12}G_2$ is consistent with the fact that the β-anomer is linear and extends in the solvent, whereas the α-anomer is more folded, and hence constrained on the micelle surface. In all cases, the $\langle l_{pl} \rangle$ values are within 1 Å of the experimental values estimated from SAXS and SANS experiments, i.e., 5.4 ± 0.1 and 6.2 ± 0.1 Å for α-$C_{12}G_2$ and β-$C_{12}G_2$, respectively.[13,76]

C. Density Profiles of the Micelles. To compare the spatial extent of the most relevant atomic group components of the micelles, we have computed their average radial mass density profiles $\rho(r)$ as a function of the distance, r, of the group from the center of mass (COM) of the micelle.[79] We discuss here the $\rho(r)$ values obtained for the entire micelle (Micelle), the maltose headgroup (Maltose), the dodecane tail (DOD), the two maltose glucose rings (GlcA and GlcB), and the hydration water (H_2O). As previously discussed,[79] the nonspherical nature of the micelles will affect the $\rho(r)$ value to a certain extent, causing the broadening of these functions. $\rho(r)$ values, averaged over the last 11 ns of each trajectory, are shown in Figure 5. The hydrophobic core $\rho(r)$ profiles extend from 0 to ~19.0 Å from the micelle COM, and present similar shapes regardless of the force field. For the hydrophilic maltose head, the $\rho(r)$'s present a strong peak with density maxima at 21.0 ± 0.5 and 25.0 ± 0.5 Å for the α- and β-$C_{12}G_2$ micelles, respectively. These values are close to those obtained previously for $\langle R_g \rangle$. We notice that the position of the main peaks for the GlcA and GlcB density profiles depends more strongly on the force field than that of the other groups studied here. Considering all the results, GlcA $\rho(r)$'s extend from 15.0 to 25.0 Å and from 18.0 to 28.0 Å for α- and β-$C_{12}G_2$ micelles, respectively. Larger values, of 1−2 Å, are found for all GlcB $\rho(r)$ values. The water density profile in Figure 5 shows that water molecules deeply penetrate into the micelle headgroup and solvate the maltose heads to a different degree with a preference for the outermost glucose ring (GlcA). We can also emphasize that water shares significant contact with the micelle hydrophobic core, as seen by the intercepts of the water and DOD $\rho(r)$ curves. Finally, the water $\rho(r)$ curves reach their bulk density value (~1.0 g/cm^3) near the edge of the box at 35 Å (α-$C_{12}G_2$) and 38 Å (β-$C_{12}G_2$) from the micelle COM.

TABLE 3: Surface Properties of the Micelles[a]

force field	micelle	$\langle SA_{HG}^{C_{12}G_2}\rangle$	$\langle SA_{v}^{C_{12}G_2}\rangle$	$\langle SA_{e}^{C_{12}G_2}\rangle$	$\langle f_{tail}\rangle$
CHARMM-K	α-$C_{12}G_2$	61.1	19425.0	9244.5	11.0
	β-$C_{12}G_2$	65.1	33237.6	16581.5	10.0
CHARMM-Opt	α-$C_{12}G_2$	60.4	17625.0	9013.2	10.9
	β-$C_{12}G_2$	56.8	29422.8	15894.6	9.3
GLYCAM06	α-$C_{12}G_2$	60.3	15675.0	9146.6	9.8
	β-$C_{12}G_2$	55.5	25726.8	15666.0	9.3

[a] ⟨...⟩ stands for the ensemble average. $SA_{HG}^{C_{12}G_2}$ (in Å^2) is the average surface area per headgroup computed using the micelle oil core radius. $SA_{v}^{C_{12}G_2}$ and $SA_{e}^{C_{12}G_2}$ are the average micelle surfaces computed with the Voronoi polyhedron,[90] assuming an ellipsoid-like geometry for the micelle. $\langle f_{tail}\rangle$ is the average surface fraction shared between the water and the $C_{12}G_2$ alkyl chain. The statistical errors (maximum errors) are always lower than 3.0 and 0.2% for the surfaces and $\langle f_{tail}\rangle$ values.

TABLE 4: Hydration Numbers[a]

	CHARMM-K		CHARMM-Opt		GLYCAM06	
system	α-$C_{12}G_2$	β-$C_{12}G_2$	α-$C_{12}G_2$	β-$C_{12}G_2$	α-$C_{12}G_2$	β-$C_{12}G_2$
$\langle n_w^{G_2}\rangle$	8.3	8.6	8.2	7.6	7.6	7.2
$\langle n_w^{GlcA}\rangle$	5.2	5.6	5.2	5.1	4.7	4.9
$\langle n_w^{GlcB}\rangle$	3.1	3.0	3.0	2.5	2.9	2.3
$\langle n_w^{C_{12}}\rangle$	0.8	0.8	0.8	0.7	0.6	0.6
$\langle n_w^{C_{12}G_2}\rangle$	9.1	9.4	9.0	8.3	8.2	7.8

[a] ⟨...⟩ stands for the ensemble average. $\langle n_w^{G_2}\rangle$, $\langle n_w^{GlcA}\rangle$, $\langle n_w^{GlcB}\rangle$, $\langle n_w^{C_{12}}\rangle$, and $\langle n_w^{C_{12}G_2}\rangle$ give the average number of water molecules at 4.0 Å of the maltose head, the outermost and innermost glucose rings, and the alkyl chain, respectively. The statistical errors (maximum errors) are always lower than 0.1%.

D. Hydration of the Headgroup. As discussed in the previous section, radial mass density profiles show significant interaction between water and the $C_{12}G_2$ surfactant headgroups. To gain insight on this aspect, we provide in Table 3 some surface area (SA) properties of the micelles computed from the last 11 ns of the simulations. We first compare the instantaneous value of the SA per surfactant headgroup ($SA_{HG}^{C_{12}G_2}$) with the results of Dupuy et al.[13] obtained from SAXS and SANS experiments assuming that the α- and β-micelles are spherical. As described by these authors $SA_{HG}^{C_{12}G_2}$, the surface of the hydrophobic core of a sphere of radius $\bar{R}^{HC}$ was calculated. The average ellipsoid semiaxes of the micelle hydrophobic core $\langle a_{HC}\rangle$, $\langle b_{HC}\rangle$, and $\langle c_{HC}\rangle$ were used to calculate $\bar{R}^{HC}$ with the expression $\bar{R}^{HC} = (\langle a_{HC}\rangle\langle b_{HC}\rangle\langle c_{HC}\rangle)^{1/3}$. The average values of $SA_{HG}^{C_{12}G_2}$ ($\langle SA_{HG}^{C_{12}G_2}\rangle$) are reported in the third column of Table 3. We found that the $\langle SA_{HG}^{C_{12}G_2}\rangle$ values are in the range 60.3−61.1 and 55.5−65.1 Å^2 for the $C_{12}G_2$ α- and β-anomers, respectively. The values obtained with CHARMM-Opt and GLYCAM06 agree well with the experimental values (58 and 52 Å^2 for the $C_{12}G_2$ α- and β-anomers, respectively), whereas the CHARMM-K results are further away.

In the fourth and fifth columns of Table 3 are reported the average surface areas (SA) for the whole micelles $\langle SA_{v}^{C_{12}G_2}\rangle$ and $\langle SA_{e}^{C_{12}G_2}\rangle$, respectively. The $SA_{v}^{C_{12}G_2}$ values were obtained from the Voronoi construction[90] by adding up the surface areas of each Voronoi polyhedron shared between all surfactant atoms and water.[91] Instead, $SA_{e}^{C_{12}G_2}$ is the ellipsoidal surface of the micelle obtained from the average semiaxis lengths ($\langle a_M\rangle$, $\langle b_M\rangle$, and $\langle c_M\rangle$) computed in section III.B. Comparison of the two values confirms that the micelle interfaces are corrugated (as also shown in Figure 1). Indeed, the surface rugosity factors $f_s = SA_{v}^{C_{12}G_2}/SA_{e}^{C_{12}G_2}$ were calculated between 1.7 and 2.1 and between 1.64 and 2.0 for the α- and β-anomers, respectively.

In the sixth column of Table 3, we also provide the average $C_{12}G_2$ surface alkyl chain ratio of the micelles, $\langle f_{tail}\rangle$, in contact with the solvent. The $\langle f_{tail}\rangle$ values were calculated with the $SA_{v}^{C_{12}G_2}$ and the surface area of the alkyl chain atoms, $SA_{v}^{C_{12}}$. $\langle f_{tail}\rangle$ values for all the micelles decrease by ∼1.0% when the surfactant head changes from the α- to the β-anomer and are calculated between 9.8 and 11.1% and between 9.3 and 10% for the α- and β-anomers, respectively. The lower $\langle f_{tail}\rangle$ values of GLYCAM06 indicate that for those micelles the surfactant alkyl chains of the micelle are more protected from the solvent than those obtained in the simulations with the CHARMM force fields. In comparison, the $\langle f_{tail}\rangle$ values reported in this work are lower than those found by Stephenson et al.[51] for a micelle with 45 β-$C_{12}G_2$ (∼17.0%), and also lower than those for micelles with 27 octyl-β-galactose[47] (∼30%) and 92 octyl-β-glucose monomers (20%).[46] The latter is probably due to the smaller size of the headgroup in those micelles, which shields less the micelle hydrophobic core from water.

The values of the average number of water molecules, $\langle n_w\rangle$, in the first solvation shell of each surfactant, or hydration number, were also computed during the last 11 ns of each run. They are presented in Table 4. For each configuration, the hydration water molecules were selected using a simple cutoff radius criterion, as described in ref 92. Briefly, a water molecule is considered near the micelle surface if its distance with any of the detergent atoms is less than $R_{cut} = f(R_w + R_{C_{12}G_2})$, where R_w and $R_{C_{12}G_2}$ are the force field van der Waals radii of the water and of the $C_{12}G_2$ atoms, respectively. f is a parameter set arbitrarily to 1.1 in our calculations.[92] Five hydration numbers were calculated here: for the whole $C_{12}G_2$ molecule ($\langle n_w^{C_{12}G_2}\rangle$), for the headgroup ($\langle n_w^{G_2}\rangle$), for the GlcA ($\langle n_w^{GlcA}\rangle$) and GlcB ($\langle n_w^{GlcB}\rangle$) units, and for the alkyl chain ($\langle n_w^{C_{12}}\rangle$). For all $\langle n_w\rangle$'s, higher values are found for the simulations obtained with CHARMM-K, whereas the $\langle n_w\rangle$'s of CHARMM-Opt and GLYCAM06 simulations are close to one another. The $\langle n_w^{G_2}\rangle$ values for CHARMM-Opt and GLYCAM06 are computed around 8.2 and 7.2, respectively, and compare well with the estimation of $\langle n_w^{C_{12}G_2}\rangle$ obtained from SANS, SAXS (8.0),[13] or TRFQ experiments for β-$C_{12}G_2$ micelles (7.9).[75] The bent conformation of the α-$C_{12}G_2$ slightly increases the headgroup hydration by 0.4−0.6 waters for the micelles simulated with the CHARMM-Opt and GLYCAM06 parameters, whereas for CHARMM-K the $\langle n_w^{G_2}\rangle$ decreases by 0.3 units. For maltose molecules in water, hydration numbers between 5.7 and 22.6 are estimated by experimental studies, whereas values within 6.5−14.5 are obtained from computer simulations (see Table 3 of ref 33 and references therein). The validity of these results depends on the experimental techniques or the force field considered. Comparison of the hydration of the glucose rings GlcA and GlcB shows that the number of water molecules around GlcB, connected to the alkyl chain, is, on average, ∼2.6 units lower than that for GlcA. This is independent of the force field employed and the conformation of the headgroup. Finally, the low values for $\langle n_w^{C_{12}}\rangle$ (<1.0 water) confirm that the micelle hydrophobic core only has sporadic contacts with the solvent consistently with the $\langle f_{tail}\rangle$ value calculated in this work.

To further examine the headgroup hydration, in Table 5, we provide the average number of nearest waters for each maltose-oxygen, or $\langle n_{Ox-Ow}\rangle$, obtained from the computed radial pair density functions (RDFs) of the maltose-oxygen (O_{1-10}) and water-oxygen (O_w) atoms. To obtain $\langle n_{Ox-Ow}\rangle$ the RDF functions were integrated until the first minimum at $r \approx 3.5$ Å after the first peak. The $\langle n_{Ox-Ow}\rangle$ results indicate that water molecules solvate primarily the hydroxyl oxygen atoms (O_1, O_2, O_3, O_4, O_6, O_8, O_9, and O_{11}) of the maltose headgroup. This is consistent

TABLE 5: Nearest Neighbors for the Maltose Oxygens[a]

	CHARMM-K			CHARMM-Opt			GLYCAM06		
$\langle n_{Ox-Ow}\rangle$	α-$C_{12}G_2$	β-$C_{12}G_2$	$\Delta_{\alpha\to\beta}$	α-$C_{12}G_2$	β-$C_{12}G_2$	$\Delta_{\alpha\to\beta}$	α-$C_{12}G_2$	β-$C_{12}G_2$	$\Delta_{\alpha\to\beta}$
O_1-O_w	0.7	0.8	0.1	0.5	0.5	0.0	0.5	0.4	−0.1
O_2-O_w	2.3	2.7	0.4	2.5	2.3	−0.2	2.1	2.6	0.5
O_3-O_w	3.6	3.7	0.1	2.9	3.2	0.3	3.0	3.4	0.4
O_4-O_w	2.0	2.6	0.6	2.3	2.6	0.3	1.9	2.4	0.5
O_5-O_w	1.1	1.3	0.2	1.3	1.0	−0.3	1.3	1.0	−0.3
O_6-O_w	3.1	2.5	−0.6	2.6	2.3	−0.3	3.2	2.4	−0.8
total GlcA	**12.8**	**13.6**	**0.8**	**12.1**	**11.9**	**−0.2**	**12.0**	**12.2**	0.2
O_7-O_w	0.2	0.5	0.3	0.3	0.3	0.0	0.2	0.4	0.2
O_8-O_w	2.4	1.9	−0.5	1.9	1.6	−0.3	1.7	1.5	−0.2
O_9-O_w	2.4	2.0	−0.4	2.2	1.8	−0.4	2.2	1.6	−0.6
$O_{10}-O_w$	0.8	0.9	0.1	0.7	0.6	−0.1	0.6	0.8	0.2
$O_{11}-O_w$	2.0	1.7	−0.3	1.7	1.6	−0.1	1.8	1.3	−0.5
total GlcB	**7.8**	**7.0**	**−0.8**	**6.8**	**5.9**	**−0.9**	**6.5**	**5.6**	**−0.9**

[a] The micelle oxygen atoms are labeled as follows: O_1 and O_7 are the acetalic oxygens, O_5 and O_{10} are the maltose ring oxygens, and all the remaining are hydroxyl oxygens (see Figure 1). Also, $\Delta_{\beta-\alpha}$ is the difference in the average number of nearest neighbors between the β- and α-anomers. The values have been obtained by integrating the O_x-O_w pair correlation functions $g(r)$ up to the first minimum at around $r \approx 3.5$ Å. Total GlcA and total GlcB give the average nearest neighbors for the outermost and innermost glucose unit of the molecule, respectively.

with previous simulation studies performed on other glycolipid micelles.[44,46,47] The number of water molecules in the first shell of these atoms is found to be between 1.9 and 3.7 as a function of the oxygen localization on the headgroup. These values vary little with the force field employed and the surfactant conformation. In general, the higher $\langle n_{Ox-Ow}\rangle$ values are obtained for the oxygen atoms O_3 (2.9−3.4) and O_6 (3.2−2.4), the most the atoms are exposed to the solvent in GlcA. As an example, the hydroxyl oxygen O_{11} in GlcB has about one water molecule in its first shell that the equivalent hydroxyl oxygen atom O_6 in GlcA. The hydration of the ring oxygen atoms O_5 and O_{10} of GlcA and GlcB does not change much (∼0.3 water) when the surfactant conformation changes from the α- to β-anomer. Finally, for the oxygen atoms involved in the glycosidic bond (O_1) and the link between the headgroup and alkyl chain (O_7), low $\langle n_{Ox-Ow}\rangle$ values (<0.8 and <0.5) are found, indicating that these oxygens are shielded from the solvent. This result is also consistent with another study,[46] where a $\langle n_{Ox-Ow}\rangle$ value close to 0.2−0.3 for O_7 was observed.

Considering the strong interaction between the $C_{12}G_2$ headgroup atoms and water, it is clear that the headgroup oxygen atoms will form an extended network of hydrogen bonds with water molecules and with donor groups of the detergent themselves.[93] The average number of HBs between water molecules and the maltose headgroup (WHB) and within the surfactant headgroups (HHB) were computed for the last 11 ns of the simulations, using the following geometrical criterion: a HB was considered if the oxygen−oxygen distance equals or is smaller than 3.5 Å and the angle O−H···O was between 120 and 180°.[94] These values are reported in Tables S4, S5, and S6 of the Supporting Information. We observed that each α-$C_{12}G_2$ molecule presents 0.5−1.0 more WHB than the β-anomer. These values vary only slightly with the force fields, with CHARMM-K having the largest number of HBs in α-$C_{12}G_2$ followed by CHARMM-Opt and GLYCAM06. This result is in agreement with small variations of hydration water in the first shell of the $C_{12}G_2$ headgroup and the decrease of $\langle n_{Ox-Ow}\rangle$ reported in the previous paragraph. We found that each $C_{12}G_2$ headgroup makes, on average, ∼1.5 times more in the establishment of HB as an acceptor (∼7.0) than as a donor (∼5). This is consistent with previous computer simulation studies of C_8G_1 and C_8Gal in water.[47] As also expected, the total number of WHBs obtained in this work is lower than the total WHBs found for maltose in TIP3P water where the number of WHBs is ∼15.9 and 22.4.[27,32] Further analysis of the individual HB donors and acceptors shows that the O_3 and O_6 (GlcA) and O_8 and O_9 (GlcB) hydroxyl oxygens make about one additional HB with water than the other oxygens. For these same oxygens, the number of WHBs decreases by ∼0.2 when the headgroup changes from the α- to the β-anomer. Finally, due to the strong entanglement of the maltose head at the micelle surface and to the low hydration of some of the hydroxyl oxygen atoms, it is expected that a large network of inter- and intra-headgroup donor/acceptor HBs (INHBs and INTHBs, respectively) will be favored. Several inter-headgroup HBs have been computed (among these previously examined by Chong et al.[47]) and are reported in the fifth to ninth columns in Tables S4, S5, and S6 in the Supporting Information. The number of INHBs is found to be much lower than the number of solvent-headgroup HBs. On average, there are ∼0.10 and ∼0.25 HBs per lipid for structures obtained from the CHARMM and GLYCAM force field simulations, respectively. The number of INHBs is greater in β-$C_{12}G_2$ micelles and is mostly due to the $O_6-H\cdots O_4$, $O_8-H\cdots O_{10}$, and $O_8-H\cdots O_9$ HBs. Furthermore, three other INTHBs were previously observed ($O_6H_6\cdots O_5$ and $O_{11}H_{11}\cdots O_{10}$ in the first and second glucose rings and $O_2H_2\cdots O_9$ between GlcA and GlcB).[27,28,94] These HBs are correlated with the rotational freedom of the ω torsion angles and the α(1→4) glycosidic linkage flexibility. Our calculations indicate that these HB types exist during all of the simulations. In particular, $O_2H_2\cdots O_9$ is present during approximately 70−80% of the simulation times, whereas the two other INTHBs only ∼30−40% of the time.

E. Conformation of the Surfactant. To examine in more detail the hydration differences of the micelles, we have studied the surfactant conformation by computing the main peak of the average end-to-end distance probability distributions $P(r)$. Specifically, we have computed $d_{C_{12}}$ and d_{G_2} by collecting from the trajectories the distances between the atoms C_7 and C_{19} of the alkyl chain and between the O_4 and O_{12} of the maltose head, respectively. Since the $d_{C_{12}}$ and d_{G_2} end-to-end distances are strongly related to the conformations of the alkyl tail and headgroup of the surfactant, respectively, we have examined the conformation of several characteristic torsion angles of the tail (such as all the CCCC dihedral angles, the first $C_7C_8C_9C_{10}$, and last $C_{15}C_{16}C_{17}C_{18}$ dihedrals),[44] the torsion angles involved in the connection of the alkyl chain and the maltose head (i.e., $O_7C_7C_8C_9$,[44] $O_{10}C_1'O_7C_7$,[27,95] and $C_1'O_7C_7C_8$[28,96]), and ω1 and

TABLE 6: Trans and Gauche Populations[a]

	CHARMM-K		CHARMM-Opt		GLYCAM06	
micelle	α-$C_{12}G_2$	β-$C_{12}G_2$	α-$C_{12}G_2$	β-$C_{12}G_2$	α-$C_{12}G_2$	β-$C_{12}G_2$
CCCC	71.8, 28.2[a]	72.0, 28.0[a]	71.4, 28.6[a]	72.1, 27.9[a]	84.6, 15.4[a]	84.7, 15.3[a]
$C_7C_8C_9C_{10}$	67.4, 32.6[a]	70.9, 28.1[a]	66.7, 33.3[a]	67.7, 32.3[a]	82.0, 18.0[a]	80.0, 20.0[a]
$C_{15}C_{16}C_{17}C_{18}$	73.3, 26.7[a]	75.4, 24.6[a]	70.8, 29.2[a]	68.5, 31.5[a]	81.0, 19.0[a]	82.8, 17.2[a]
$O_7C_7C_8C_9$	80.5, 20.5[a]	80.6, 20.4[a]	54.4, 46.6[a]	53.3, 47.7[a]	61.8, 38.2[a]	63.0, 37.0[a]
$O_{10}C_1'O_7C_7$	2.3, 97.7[b]	0.1, 99.9[c]	0.5, 99.5[b]	4.9, 95.1[c]	2.4, 97.6[b]	6.7, 93.3[c]
$C_1'O_7C_7C_8$	90.1, 8.9[a]	89.1, 10.9[a]	71.7, 28.3[a]	76.4, 23.6[a]	81.7, 18.3[a]	78.1, 11.9[a]
$O_6C_6C_5O_5$ (ω_1)	59.0[b], 43.7[c]	59.3[b], 39.4[c]	60.9[b] 35.0[c]	51.6[b], 39.3[c]	51.7[b], 44.7[c]	50.9[b], 44.5[c]
$O_{11}C_6C_5O_{10}$ (ω_2)	24.5[c], 75.3[c]	37.0[b], 54.4[c]	36.7[b], 60.0[c]	29.9[b], 26.7[c]	30.9[b], 65.9[c]	37.1[b], 53.9[c]

[a] Dihedral angles between −180 and −120°, between −120 and +120°, and between +120 and +180° are defined as gauche$^+$ (p_g^+), trans (p_t), and gauche$^-$ (p_g^-), respectively. The exponents a, b, and c are for [a]gauche^{+-}, [b]gauche$^+$, and [c]gauche$^-$, respectively. The statistical errors (maximum errors) are always lower than 0.3%. See the main text for details.

ω2 angles (i.e., $O_6C_6C_5O_5$[95] and $O_{11}C_6C_5O_{10}$[64]) by computing the corresponding normalized dihedral angle distribution $P(\phi)$. These functions were computed and averaged over the last 11 ns of each run. The relative gauche^{+-} (p_g^{+-}) and *trans* (p_t) populations were also extracted and are presented in Table 6. $P(r)$ functions for the two CHARMM simulations (not shown here) display similar shapes with a strong peak at $d_{C_{12}} \approx 12.3$ Å for all the micelles regardless of the surfactant headgroup anomer. This is ∼10.9% smaller than the value (∼14.0 Å) calculated for an extended dodecane chain with the modeling program Discovery Studio Visualizer. In contrast to the CHARMM results, the alkyl tail $P(r)$ functions for the two micelles simulated with GLYCAM06 parameters present two peaks at $d_{C_{12}} \approx 13.0$ Å and $d_{C_{12}} \approx 13.8$ Å (figures not shown), indicating a coexistence of two populations for the alkyl chain length. In the literature, a smaller value for $d_{C_{12}}$ is strongly related to the partial folding of the hydrophobic chain in the micelle core and existence of "*gauche defaults*".[97,98] In this context, we found that the CCCC dihedral angles of the alkyl chain are mostly in their *trans* state with relative populations p_t close to 72.0 and 84.6% for the CHARMM and GLYCAM06 force fields, respectively. These results are consistent with previous simulations of micelles containing surfactant with a dodecane chain (see, for instance, refs 59, 99, and 100). As for the CHARMM simulations, the peaks in $P(r)$ peaks do not change much (<1%) when going from an axial (α-) to an equatorial (β-) conformation of the surfactant headgroup (see Table 6). Further investigation shows that the outermost and innermost CCCC dihedral angles (i.e., $C_7C_8C_9C_{10}$ and $C_{15}C_{16}C_{17}C_{18}$) have a larger gauche^{+-} population, $p_g^{+-} \approx 27\%$, than the others dihedrals in the alkyl chain, $p_g^{+-} \approx 15\%$. Similar results were found in previous MD simulations of octyl-β-glucoside micelles,[44] where the lower steric conflicts found at the extremities of the alkyl chains decrease the gauche conformation of the chain. Finally, we find only small differences, less than 12% in p_t, in the CCCC angles between the CHARMM and GLYCAM06 simulations. Similar behaviors were obtained in simulations of LDAO micelles simulated with the CHARMM27 and AMBER94 force fields, $p_t \approx 71.0\%$ and $p_t \approx 82.8\%$, respectively.[101]

In our simulations, the $O_7C_7C_8C_9$ dihedral angle remain in a *trans* state, in agreement with previous simulations of octyl-β-glucoside micelles.[44] Nevertheless, we found that CHARMM-Opt has a p_g^{+-} value 25% smaller than that of CHARMM-K, closer to GLYCAM06, and in agreement with QM/MM calculations carried for the α- and β-anomers of maltose.[67] For the $O_{10}C_1'O_7C_7$ (Φ) dihedral angle, we observed that, for all the simulations, this angle is in gauche$^+$ (>∼90%) for the α- and β-anomers. Also, our results show that for all the micelles the Ψ dihedral angle, $C_1'O_7C_7C_8$, is always found in a *trans* state. Compared to CHARMM-K, in CHARMM-Opt, the p_t value of this angle decreases by ∼13 units to 18% depending on the anomer, and is closer to the values obtained for the GLYCAM force field.

In the last two rows of Table 6, we have listed for all the simulations the average relative population of the two ω dihedral angles in the reducing (GlcA) ($\omega_1 = O_6C_6C_5O_5$) and nonreducing (GlcB) ($\omega_2 = O_{11}C_6'C_5'O_{10}$) glucose units of the maltose head. In glucopyranose, due to rotational freedom of the ω dihedral angle, three stable conformers exist, defined by the position of the OH oxygen relative to oxygen ring atoms (here, O_5 and O_{10}), termed *gauche−gauche (gg), gauche−trans (gt),* and *trans−gauche (tg)* which correspond to ω = −60, −60, and 180°.[102−104] Computational results on maltose have shown that ω has a strong preference for gauche values.[58,105] This is due to steric repulsions between the hydroxyl groups in position 4 and 6, described as the "gauche effect".[106]

In contrast to maltose in vacuum, where the ω angle adopts preferentially a *gt* conformation, for maltose in solution, MD simulations performed in condensed phase[28,37] and experimental studies[107] have shown that the *gg* conformation is favored. Our results for CHARMM-K and CHARMM-Opt show a different behavior for ω, for which the conformation *gt* is favored with respect to *gg* (*gt*/*gg* ≈ 60:40). For GlcB, we find that these angles are mainly in the *gg* conformation except for the β-anomer where ω_2 has highly similar *gg* and *gt* populations. These results can be explained by the incomplete hydration of the maltose headgroup in the detergent and the existence of intermaltose HBs.

Turning our attention to the maltose head linkage conformation, the $P(r)$ functions (not shown here) present peaks at $d_{G_2} \approx 8.8$ Å (α-anomer) and $d_{G_2} \approx 9.8$ Å (β-anomer). These values change slightly (0.2 Å) with the potential employed and are smaller than the length for a maltose molecule in an elongated conformation (10.3 Å, with $\Phi_H = \Psi_H = 0.0°$). In Figure 6, we have plotted the distribution maps of the $P(\Phi_H,\Psi_H)$ glycosidic dihedral angle pair in population percentage for all simulations. We find that, except for the α-$C_{12}G_2$ micelle simulated with the new CHARMM potential, all of the $P(\Phi_H,\Psi_H)$ present a compact elliptic shape with a maximum point near (−40°, −25°) ± 10°. In the former system, instead, two areas are sampled, around (−25°; −20°) and (−65°; −50°), for 70% and 30% of the total simulation time, respectively. It is difficult to validate these results, as no experimental data exist in the literature for $P(\Phi_H,\Psi_H)$ of $C_{12}G_2$ micelles and these results differ for a maltose molecule in water where experimental (such as NMR[32,38,108,109] or optical rotation[110]) and theoretical studies

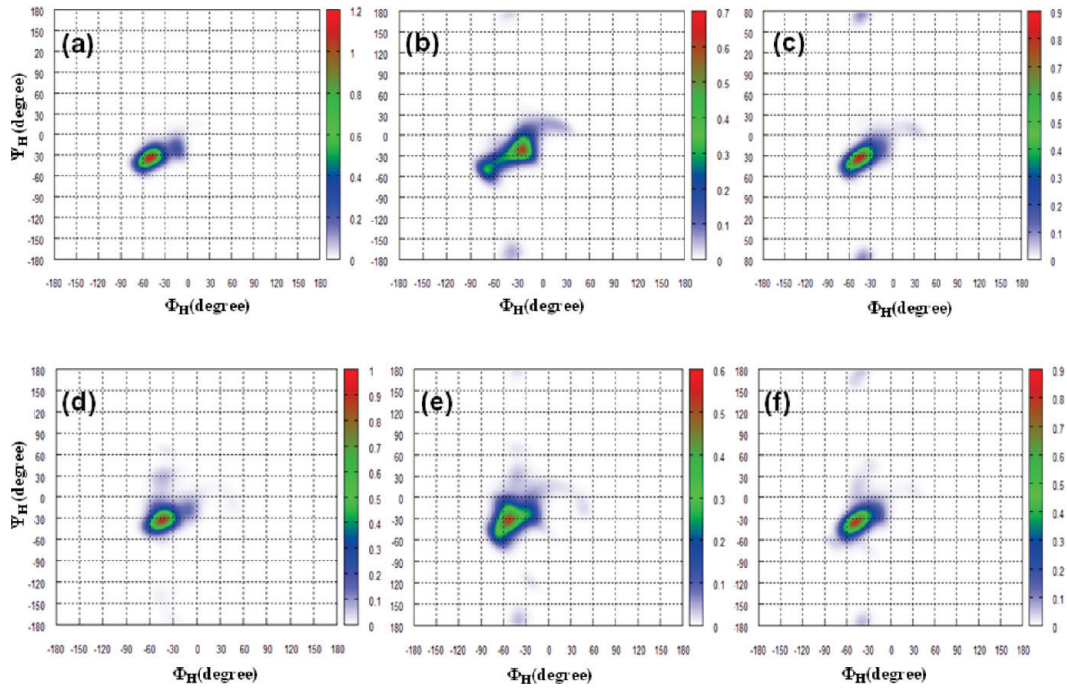

Figure 6. Distribution map of the Φ_H/Ψ_H glycosidic dihedral angle pairs in population percentage for α- (a) and β-anomers (b) of $C_{12}G_2$ micelles for the CHARMM-K (a and d), CHARMM-Opt (b and e), and GLYCAM06 (c and f) force fields, respectively. The grid interval is 5.0°, and the contour lines are spaced every 0.2%.

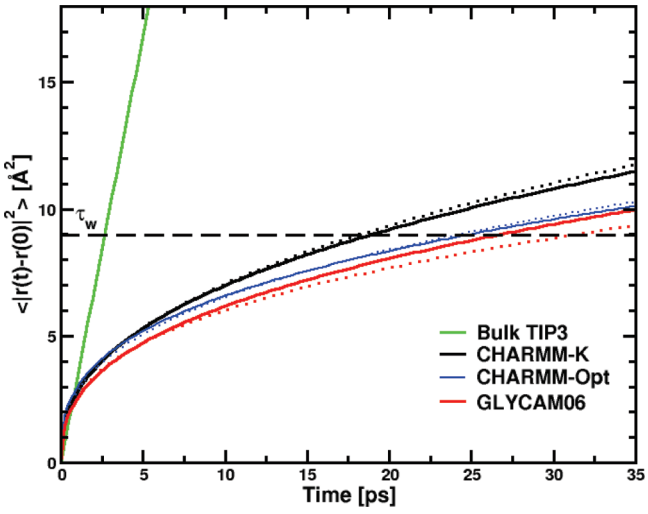

Figure 7. Interfacial water mean square displacement (MSD) as a function of time for α- (continuous line) and β-anomers (dotted line). The black dashed line gives the distance for computing the residence time τ_w (see the main text).

(such as QM[38,111,112] and MD[28,32,37,69,113]) predicted two peaks for $P(\Phi_H,\Psi_H)$ around (−50°; −30°) ± 20° and (−40°; −30°) ± 20°.

F. Water Dynamics at the Micelle Surface. To examine the dynamic behavior of water molecules around the micelles, we have computed the mean square displacement (MSD) of the translational diffusion $\langle|r(t) - r(0)|^2\rangle$ for water molecules at the micelle surface. Water molecules included in this calculation were at a distance of less than 4.0 Å from any detergent molecule at a given time of the trajectory (details about the calculation are available in ref 47). For the different micelles studied in this work, the MSD functions are shown in Figure 7 and the translational diffusion parameters are reported in Table 7. MSD functions are compared with the results obtained from a NPT simulation (T = 297 K and P = 0.1 MPa) for 1000 TIP3 water molecules simulated in a cubic box for 1 ns. As shown previously for water molecules near protein surfaces,[114,115] direct micelles,[116,117] or reverse micelles,[79,118] the water MSD presents a subdiffusive regime and can be fitted with a power law (i.e., $\langle|r(t) - r(0)|^2\rangle \propto t^\theta$) rather than a linear dependence in time as observed in bulk water. This behavior is assumed to be the consequence of the geometric/energetic disorder found at the micelle and protein surfaces.[114] For all micelles, the fit to a power law leads to similar values for θ, around 0.34 and 0.40. These values are comparable to the θ values found previously by one of us (M.M.) for water around the $C_{12}E_6$ micelle surface (0.3 and 0.4 at T = 283 and 318 K, respectively).[117] In this micellar system, it has been shown that the water interacts with the long hydrophilic ethylene oxide $(EO)_{15}$ chain through a large hydrogen bond network.[119] For a subdiffusive regime, it is useful to define a rough estimate of the water residence time, τ_w, as the time needed by a water molecule to cover a distance of 9 Å^2, i.e., corresponding to a path spanning a water molecular diameter.[120] The ratios between τ_w and the residence time of the bulk water values (τ_w^b = 2.7 ps) are reported in the fourth and fifth rows in Table 7. We find that the τ_w values change significantly with the force field employed but not with the surfactant headgroup conformation. τ_w values are calculated for all the simulations between 18.9 and 30.5 ps. In the GLYCAM06 simulations, water dynamic retardation, or τ_w^b/

TABLE 7: Translational Diffusion of the Hydration Waters[a]

	CHARMM-K		CHARMM-Opt		GLYCAM06	
system	α-$C_{12}G_2$	β-$C_{12}G_2$	α-$C_{12}G_2$	β-$C_{12}G_2$	α-$C_{12}G_2$	β-$C_{12}G_2$
θ	0.39	0.40	0.34	0.36	0.38	0.35
τ_w (ps)	18.9	18.3	24.8	24.8	27.2	30.5
τ_w/τ_w^b	6.7	6.5	8.5	8.5	11.7	11.3

[a] θ is the dispersion regime parameter obtained by fitting the $\langle|r(t) - r(0)|^2\rangle$ function to t^θ. τ_w is the water residence time, defined as the time (in ps) for a water to cover a distance equal to its own diameter (i.e., 3 Å), and τ_w/τ_w^b is the retardation or the ratio between the water residence time in the micelle and the bulk.

τ_w, is ~11.3 for the α-anomer and 11.7 for the β-anomer. The differences obtained for water diffusion is probably the result of the headgroup conformation variations and the number of trapped water molecules at the micelle interface for the six micelles.

To the best of our knowledge, no experimental data on water dynamics are available for $C_{12}G_2$ micelles. Notwithstanding, Chong et al.[47] have computed the residence time of water near each headgroup oxygen atom for micelles of octyl-glucose (C_8G_1) and galactose (C_8Gal). The authors found that τ_w maximum values are between 41.0−164.0 ps (C_8G_1) and 28.4−88.0 ps (C_8Gal) depending on the localization of the hydroxyl group in the headgroup and the cutoff employed. The largest τ_w values are found for water molecules trapped within the crevices and clefts at the micelle surface. Finally, the τ_w values obtained here largely exceed the average residence time found by MD for water in the first shell of maltose (~11.6 ps) in water[31] or in QENS experiments at 320 K (~3.4 ps).[121]

IV. Conclusion

In this paper, we have presented the development of two new potential models, based on the CHARMM36 and GLYCAM06 force fields, to be used in the molecular modeling of the α- and β-anomers of $C_{12}G_2$ GL. These surfactants are widely employed to extract and solubilize membrane proteins. To validate these potentials, we have investigated the structure of significant $C_{12}G_2$ micelles by MD simulations. In particular, we have studied the structural properties of the micelles with the two anomeric forms, and described the dynamical properties of water molecules at the micelle/water interface. The results obtained for the new potentials were also compared with those obtained with older parameters developed for carbohydrate for CHARMM22.

We found that the three force fields studied here lead to different results particularly for the properties related to the headgroup conformation and micelle hydration. In particular, our calculations show that the α- and β-$C_{12}G_2$ micelles have a $\langle R_g \rangle$ value close to 20.2 and 25.4 Å, respectively. The computed $\langle R_g \rangle$'s agree reasonably well with SAXS and SANS experiments[13] when the micelles are simulated with the new parameters developed for CHARMM36, CHARMM, and GLYCAM06.

Concerning the global shape of the micelles, we observed no significant differences between the three force fields and the different micelles studied. The α-$C_{12}G_2$ micelles have an average major-to-minor semiaxis ratio $\langle a_M/c_M \rangle$ close to 1.20, whereas the β-$C_{12}G_2$ micelles have a more pronounced oblate shape with $\langle a_M/c_M \rangle$ values around 1.38−1.43, in qualitative agreement with published experimental observations.[13,26,75] The computed radial density profiles indicate that water penetrates deeply at the micelle headgroup and hydrates preferentially the outermost glucose ring (GlcA). Due to the difference in the surfactant headgroup conformations, we also observed slight differences in the headgroup hydration. Consistent with previous simulations carried out with other glycolipid systems,[44,46,47] we found that the micelle/water interfaces are highly corrugated with rugosity factor values around 1.6−2.0. The average solvent surface areas for the α- and β-$C_{12}G_2$ anomers simulated with CHARMM-Opt and GLYCAM06 are found to be around 60.6 and 55.5 Å^2 per molecule, respectively, which are close to experimental values.[13]

Concerning micelle hydration, we found that the alkyl chains of $C_{12}G_2$ are in all cases sturdily protected from the solvent since ~10 % of the micelle hydrophobic core is in contact with water. Due to the strong entanglement of the maltose head at the micelle surface, within each micelle, we observed a large hydrogen bond network consisting of a complex combination of inter- and intra-HBs between adjacent headgroups. HBs between water and headgroups do not depend on the headgroup conformation, as we found highly similar patterns for headgroup/water HBs for both α- and β-anomers (with only on average ~0.6 units of difference).

Finally, investigations of the dynamic behavior of the hydrating water for all the micelles show that the water translational diffusion is strongly retarded with respect to the bulk by a factor of 7.0−11.7, depending on the potential. Interestingly, the headgroup conformation does not affect the water diffusion for the three force fields examined here. In particular, water diffusion results near the micelle interface are similar for CHARMM-Opt and GLYCAM06 (~8.5 and ~11.7 smaller than for the bulk, respectively) and are ~1.5 times larger than the diffusion values obtained in CHARMM-K-based simulations

In conclusion, the molecular modeling and simulation results reported in this paper are a first and necessary step to improve our atomic level knowledge of the $C_{12}G_2$ micelles. In addition, because our potential parameters are consistent with two major protein force fields (CHARMM and AMBER), they offer a solid starting point for further studies on the interaction and aggregation of membrane proteins with $C_{12}G_2$ detergents.

Acknowledgment. This work was, in part, granted access to the HPC resources of CCRT/CINES under the allocation 2009-t2009076076 made by GENCI (Grand Equipement National de Calcul Intensif) and financial support from the NIH (GM070855) to A.D.M.

Supporting Information Available: Force field parameters, dihedral parameters for α- and β-anomer molecules, and additional figures and tables. This material is available free of charge via the Internet at http://pubs.acs.org.

References and Notes

(1) Wiegandt, H. *Glycolipids*; Elsevier Science Ltd: Amsterdam, The Netherlands, 1985.
(2) Fischer, E. *Ber. Dtsch. Chem. Ges.* **1893**, *26* (3), 2400–2412.
(3) Koeltzow, D.; Urefer, A. *J. Am. Oil Chem. Soc.* **1984**, *61*, 1651–1655.
(4) Yakimchuk, O. D.; Kotomin, A. A.; Petel skii, M. B.; Naumov, V. N. *Russ. J. Appl. Chem.* **2004**, *77*, 2001–2005.
(5) Matsumura, S.; Imai, K.; Yoshikawa, S.; Kawada, K.; Uchibor, T. *J. Am. Oil Chem. Soc.* **1990**, *67*, 996–1001.
(6) von Rybinski, W.; Hill, K. *Angew. Chem., Int. Ed.* **1998**, *37*, 1328–1345.
(7) Balzer, D.; Lüders, H. *Nonionic Surfactants: Alkyl Polyglucosides*; CRC Press: 2000; Vol. 91.
(8) Shinoda, K.; Yamanaka, T.; Kinoshita, K. *J. Phys. Chem.* **1959**, *63*, 648–650.
(9) Nilsson, P. G.; Lindman, B. *J. Phys. Chem.* **1982**, *86*, 271–279.
(10) D'Aprano, A.; Giordano, R.; Janelli, M. P.; Magazu, S.; Maisano, G.; Sesta, B. *J. Mol. Struct.* **1996**, *383*, 177–182.
(11) Nilsson, F.; Soderman, O.; Johansson, I. *Langmuir* **1996**, *12*, 902–908.
(12) Zhang, L.; Somasundaran, P.; Maltesh, C. *Langmuir* **1996**, *12*, 2371–2373.
(13) Dupuy, C.; Auvray, X.; Petipas, C.; Rico-Lattes, I.; Lattes, A. *Langmuir* **1997**, *13*, 3965–3967.
(14) Aoudia, M.; Zana, R. *J. Colloid Interface Sci.* **1998**, *206*, 158–167.
(15) Nilsson, F.; Söderman, O.; Johansson, I. *J. Colloid Interface Sci.* **1998**, *203*, 131–139.
(16) Walian, P.; Cross, T.; Jap, B. *Genome Biol.* **2004**, *5*, 215.
(17) Raman, P.; Cherezov, V.; Caffrey, M. *Cell. Mol. Life Sci.* **2006**, *63*, 36–51.
(18) le Maire, M.; Champeil, P.; Moller, J. V. *Biochim. Biophys. Acta, Biomembr.* **2000**, *1508*, 86–111.
(19) Privé, G. *Methods* **2007**, *41*, 388–397.

(20) Jastrzebska, B.; Fotiadis, D.; Jang, G.; Stenkamp, R. E.; Engel, A.; Palczewski, K. *J. Biol. Chem.* **2006**, *281*, 11917–11922.
(21) Ostermeier, C.; Harrenga, A.; Ermler, U.; Michel, H. *Proc. Natl. Acad. Sci. U.S.A.* **1997**, *94*, 10547–10553.
(22) Qin, L.; Hiser, C.; Mulichak, A.; Garavito, R. M.; Ferguson-Miller, S. *Proc. Natl. Acad. Sci. U.S.A.* **2006**, *103*, 16117–16122.
(23) Zhuang, J.; Prive, G. G.; Werner, G. E.; Ringler, P.; Kaback, H. R.; Engel, A. *J. Struct. Biol.* **1999**, *125*, 63–75.
(24) Screpanti, E.; Padan, E.; Rimon, A.; Michel, H.; Hunte, C. *J. Struct. Biol.* **2006**, *362*, 192–202.
(25) Focher, B.; Savelli, G.; Torri, G.; Vecchio, G.; McKenzie, D. C.; Nicoli, D. F.; Bunton, C. A. *Chem. Phys. Lett.* **1989**, *158*, 491.
(26) Cecutti, C.; Focher, B.; Perly, B.; Zemb, T. *Langmuir* **1991**, *7*, 2580–2585.
(27) Brady, J. W.; Schmidt, R. K. *J. Phys. Chem.* **1993**, *97*, 958–966.
(28) Ott, K.-H.; Meyer, B. *Carbohydr. Res.* **1996**, *281*, 11–34.
(29) Naidoo, K. J.; Brady, J. W. *J. Am. Chem. Soc.* **1999**, *121*, 2244–2252.
(30) Momany, F.; Willett, J. *Carbohydr. Res.* **2000**, *326*, 210–226.
(31) Hochtl, P.; Boresch, S.; Steinhauser, O. *J. Chem. Phys.* **2000**, *112*, 9810–9821.
(32) Best, R. B.; Jackson, G. E.; Naidoo, K. J. *J. Phys. Chem. B* **2001**, *105*, 4742–4751.
(33) Lerbret, A.; Bordat, P.; Affouard, F.; Descamps, M.; Migliardo, F. *J. Phys. Chem. B* **2005**, *109*, 11046–11057.
(34) Choi, Y.; Cho, K. W.; Jeong, K.; Jung, S. *Carbohydr. Res.* **2006**, *341*, 1020–1028.
(35) Ekdawi-Sever, N.; de Pablo, J. J.; Feick, E.; von Meerwall, E. *J. Phys. Chem. A* **2003**, *107*, 936–943.
(36) Dashnau, J. L.; Sharp, K. A.; Vanderkooi, J. M. *J. Phys. Chem. B* **2005**, *109*, 24152–24159.
(37) Pereira, C. S.; Kony, D.; Baron, R.; Müller, M.; van Gunsteren, W. F.; Hünenberger, P. H. *Biophys. J.* **2006**, *90*, 4337–4344.
(38) Momany, F.; Schnupf, U.; Willett, J.; Bosma, W. *Struct. Chem.* **2007**, *18*, 611–632.
(39) Gouin, S. G.; Vanquelef, E.; Garcia Fernandez, J. M.; Ortiz Mellet, C.; Dupradeau, F.-Y.; Kovensky, J. *J. Org. Chem.* **2007**, *72*, 9032–9045.
(40) Lerbret, A.; Mason, P. E.; Venable, R. M.; Cesàro, A.; Saboungi, M. L.; Pastor, R. W.; Brady, J. W. *Carbohydr. Res.* **2009**, *344*, 2229–2235.
(41) van Buuren, A. R.; Berendsen, H. J. C. *Langmuir* **1994**, *10*, 1703–1713.
(42) Sega, M.; Brocca, P.; Melchionna, S.; Vallauri, R. *J. Phys. Chem. B* **2004**, *108*, 20322–20330.
(43) Chong, T. T.; Heidelberg, T.; Hashim, R.; Gary, S. *Liq. Cryst.* **2007**, *34*, 349–363.
(44) Bogusz, S.; Venable, R. M.; Pastor, R. W. *J. Phys. Chem. B* **2000**, *104*, 5462–5470.
(45) Bogusz, S.; Venable, R. M.; Pastor, R. W. *J. Phys. Chem. B* **2001**, *105*, 8312–8321.
(46) Konidala, P.; He, L.; Niemeyer, B. *J. Mol. Graphics Modell.* **2006**, *25*, 77–86.
(47) Chong, T. T.; Hashim, R.; Bryce, R. A. *J. Phys. Chem. B* **2006**, *110*, 4978–4984.
(48) Konidala, P.; Niemeyer, B. *Biophys. Chem.* **2007**, *128*, 215–230.
(49) Chong, T. T.; Heidelberg, T.; Hashim, R.; Saadullah, G. *Liq. Cryst.* **2007**, *34*, 349–363.
(50) Branca, C.; Magazu, S.; Maisano, G.; Migliardo, P.; Tettamanti, E. *J. Mol. Struct.* **1999**, *481*, 133–140.
(51) Stephenson, B. C.; Goldsipe, A.; Beers, K. J.; Blankschtein, D. *J. Phys. Chem. B* **2007**, *111*, 1045–1062.
(52) Jorgensen, W. L.; Maxwell, D. S.; Tirado-Rives, J. *J. Am. Chem. Soc.* **1996**, *118*, 11225–11236.
(53) Kuttel, M.; Brady, J. W.; Naidoo, K. J. *J. Comput. Chem.* **2002**, *23*, 1236–1243.
(54) Reiling, S.; Schlenkrich, M.; Brickmann, J. *J. Comput. Chem.* **1996**, *17*, 450–468.
(55) Bayly, C. I.; Cieplak, P.; Cornell, W.; Kollman, P. A. *J. Phys. Chem.* **1993**, *97*, 10269–10280.
(56) Cieplak, P.; Cornell, W. D.; Bayly, C.; Kollman, P. A. *J. Comput. Chem.* **1995**, *16*, 1357–1377.
(57) Woods, R. J.; Chappelle, R. *THEOCHEM* **2000**, *527*, 149–156.
(58) Kirschner, K. N.; Woods, R. J. *Proc. Natl. Acad. Sci. U.S.A.* **2001**, *98*, 10541–10545.
(59) Sterpone, F.; Briganti, G.; Pierleoni, C. *Langmuir* **2001**, *17*, 5103–5110.
(60) Bruce, C. D.; Berkowitz, M. L.; Perera, L.; Forbes, M. D. E. *J. Phys. Chem. B* **2002**, *106*, 3788–3793.
(61) Frisch, M. J.; Trucks, G. W.; Schlegel, H. B.; Scuseria, G. E.; Robb, M. A.; Cheeseman, J. R.; Montgomery, J. A.; Vreven, T.; Kudin, K. N.; Burant, J. C.; Millam, J. M.; Iyengar, S. S.; Tomasi, J.; Barone, V.; Mennucci, B.; Cossi, M.; Scalmani, G.; Rega, N.; Petersson, G. A.; Nakatsuji, H.; Hada, M.; Ehara, M.; Toyota, K.; Fukuda, R.; Hasegawa, J.; Ishida, M.; Nakajima, T.; Honda, Y.; Kitao, O.; Nakai, H.; Klene, M.; Li, X.; Knox, J. E.; Hratchian, H. P.; Cross, J. B.; Bakken, V.; Adamo, C.; Jaramillo, J.; Gomperts, R.; Stratmann, R. E.; Yazyev, O.; Austin, A. J.; Cammi, R.; Pomelli, C.; Ochterski, J. W.; Ayala, P. Y.; Morokuma, K.; Voth, G. A.; Salvador, P.; Dannenberg, J. J.; Zakrzewski, V. G.; Dapprich, S.; Daniels, A. D.; Strain, M. C.; Farkas, O.; Malick, D. K.; Rabuck, A. D.; Raghavachari, K.; Foresman, J. B.; Ortiz, J. V.; Cui, Q.; Baboul, A. G.; Clifford, S.; Cioslowski, J.; Stefanov, B. B.; Liu, G.; Liashenko, A.; Piskorz, P.; Komaromi, I.; Martin, R. L.; Fox, D. J.; Keith, T.; Laham, A.; Peng, C. Y.; Nanayakkara, A.; Challacombe, M.; Gill, P. M. W.; Johnson, B.; Chen, W.; Wong, M. W.; Gonzalez, C.; Pople, J. A. *Gaussian 03*; Gaussian, Inc.: Wallingford, CT, 2003.
(62) Hehre, W. J.; Radom, L.; Schleyer, P. v. R.; Pople, J. A. *Ab Initio Molecular Orbital Theory*; John Wiley and Sons: New York, 1986.
(63) Dupradeau, F.-Y.; Pigache, A.; Zaffran, T.; Savineau, C.; Lelong, R.; Grivel, N.; Lelong, D.; Rosanski, W.; Cieplak, P. *Phys. Chem. Chem. Phys.* **2010**, *12*, 7821–7839.
(64) Kirschner, K. N.; Yongye, A. B.; Tschampel, S. M.; González-Outeiriño, J.; Daniels, C. R.; Lachele Foley, B.; J. Woods, R. *J. Comput. Chem.* **2008**, *29*, 622–655.
(65) Dupradeau, F.-Y.; Cézard, C.; Lelong, R.; Stanislawiak, É.; Pêcher, J.; Delepine, J. C.; Piotr, C. *Nucleic Acids Res.* **2008**, D360–D367.
(66) Guvench, O.; Greene, S. N.; Kamath, G.; Brady, J. W.; Venable, R. M.; Pastor, R. W.; MacKerell, A. D., Jr. *J. Comput. Chem.* **2008**, *29*, 2543–2564.
(67) Guvench, O.; Hatcher, E.; Venable, R. M.; Pastor, R. W.; MacKerell, A. D., Jr. *J. Chem. Theory Comput.* **2009**, *5*, 2353–2370.
(68) Vorobyov, I.; Anisimov, V. M.; Greene, S.; Venable, R. M.; Moser, A.; Pastor, R. W.; MacKerell, A. D., Jr. *J. Chem. Theory Comput.* **2007**, *3*, 1120–1133.
(69) Guvench, O.; MacKerell, A., Jr. *J. Mol. Model.* **2008**, *14*, 667–679.
(70) Ha, S. N.; Giammona, A.; Field, M.; Brady, J. W. *Carbohydr. Res.* **1988**, *180*, 207–221.
(71) Lee, H.; Venable, R. M.; MacKerell, A. D., Jr.; Pastor, R. W. *Biophys. J.* **2008**, *95*, 1590–1599.
(72) Klauda, J. B.; Brooks, B. R.; MacKerell, A. D., Jr.; Venable, R. M.; Pastor, R. W. *J. Phys. Chem. B* **2005**, *109*, 5300–5311.
(73) MacKerell, A. D., Jr.; Bashford, D.; Bellott, M.; Dunbrack, R. L.; Evanseck, J. D.; Field, M. J.; Fischer, S.; Gao, J.; Guo, H.; Ha, S.; Joseph-McCarthy, D.; Kuchnir, L.; Kuczera, K.; Lau, F. T. K.; Mattos, C.; Michnick, S.; Ngo, T.; Nguyen, D. T.; Prodhom, B.; Reiher, W. E.; Roux, B.; Schlenkrich, M.; Smith, J. C.; Stote, R.; Straub, J.; Watanabe, M.; Wiorkiewicz-Kuczera, J.; Yin, D.; Karplus, M. *J. Phys. Chem. B* **1998**, *102*, 3586–3616.
(74) Rosevear, P.; VanAken, T.; Baxter, J.; Ferguson-Miller, S. *Biochemistry* **1980**, *19*, 4108–4115.
(75) Warr, G. G.; Drummond, C. J.; Grieser, F.; Ninham, B. W.; Evans, D. F. *J. Phys. Chem.* **1986**, *90*, 4581–4586.
(76) Lipfert, J.; Columbus, L.; Chu, V. B.; Lesley, S. A.; Doniach, S. *J. Phys. Chem. B* **2007**, *111*, 12427–12438.
(77) Martínez, J. M.; Martínez, L. *J. Comput. Chem.* **2003**, *24*, 819–825.
(78) Hunenberger, P. H.; McCammon, J. A. *Biophys. Chem.* **1999**, *78*, 69–88.
(79) Abel, S.; Sterpone, F.; Bandyopadhyay, S.; Marchi, M. *J. Phys. Chem. B* **2004**, *108*, 19458–19466.
(80) Marsili, S.; Signorini, G. F.; Chelli, R.; Marchi, M.; Procacci, P. *J. Comput. Chem.* **2010**, *31*, 1106–1116.
(81) Andersen, H. C. *J. Chem. Phys.* **1980**, *72*, 2384–2393.
(82) Parrinello, M.; Rahman, A. *J. Appl. Phys.* **1981**, *52*, 7182–7190.
(83) Rahman, A.; Stillinger, F. H. *J. Chem. Phys.* **1971**, *55*, 3336–3359.
(84) Nose, S. *J. Chem. Phys.* **1984**, *81*, 511–519.
(85) Hoover, W. G. *Phys. Rev. A* **1985**, *31*, 1695–1697.
(86) Marchi, M.; Procacci, P. *J. Chem. Phys.* **1998**, *109*, 5194–5202.
(87) Essmann, U.; Perera, L.; Berkowitz, M. L.; Darden, T.; Lee, H.; Pedersen, L. G. *Chem. Phys.* **1995**, *103*, 8577–8594.
(88) Ryckaert, J. P.; Ciccotti, G.; Berendsen, H. J. C. *J. Comput. Chem.* **1977**, *23*, 327–341.
(89) Haller, J.; Kaatze, U. *ChemPhysChem* **2009**, *10*, 2703–2710.
(90) Voronoi, G. F. *J. Reine Angew. Math.* **1908**, *134*, 198–287.
(91) Procacci, P.; Berne, B. J. *Mol. Phys.* **1994**, *835*, 255–272.
(92) Marchi, M.; Sterpone, F.; Ceccarelli, M. *J. Am. Chem. Soc.* **2002**, *124*, 6787–6791.
(93) Fringant, C.; Tvaroska, I.; Mazeau, K.; Rinaudo, M.; Desbrieres, J. *Carbohydr. Res.* **1995**, *278*, 27–41.
(94) Umemura, M.; Yuguchi, Y.; Hirotsu, T. *THEOCHEM* **2005**, *730*, 1–8.
(95) Olsson, U.; Serianni, A. S.; Stenutz, R. *J. Phys. Chem. B* **2008**, *112*, 4447–4453.
(96) Cloran, F.; Carmichael, I.; Serianni, A. S. *J. Am. Chem. Soc.* **1999**, *121*, 9843–9851.
(97) Dill, K. A. *J. Phys. Chem.* **1982**, *86*, 1498–1500.

(98) Holler, F.; Callis, J. B. *J. Phys. Chem.* **1989**, *93*, 2053–2058.
(99) MacKerell, A. D., Jr. *J. Phys. Chem.* **1995**, *99*, 1846–1855.
(100) Tieleman, D. P.; van der Spoel, D.; Berendsen, H. J. C. *J. Phys. Chem. B* **2000**, *104*, 6380–6388.
(101) Marchetti, G. Ph.D. Thesis, Université Pierre et Marie Curie, 2006.
(102) Lemieux, R. U.; Martin, J. C. *Carbohydr. Res.* **1970**, *13*, 139–161.
(103) Nishida, Y.; Ohrui, H.; Meguro, H. *Tetrahedron Lett.* **1984**, *25*, 1575–1578.
(104) Marchessault, R. H.; Perez, S. *Biopolymers* **1979**, *18*, 2369–2374.
(105) Barnett, C. B.; Naidoo, K. J. *J. Phys. Chem. B* **2008**, *112*, 15450–15459.
(106) Wolfe, S. *Acc. Chem. Res.* **1972**, *5*, 102–111.
(107) Weimar, T.; Kreis, U. C.; Andrews, J. S.; Pinto, B. M. *Carbohydr. Res.* **1999**, *315*, 222–233.
(108) Rao, V. S. R.; Foster, J. F. *J. Phys. Chem.* **1963**, *67*, 951–952.
(109) Cheetham, N. W. H.; Dasgupta, P.; Ball, G. E. *Carbohydr. Res.* **2003**, *338*, 955–962.
(110) Stevens, E. S. *Biopolymers* **1992**, *32*, 1571–1579.
(111) Gould, I. R.; Bettley, H. A.-A.; Bryce, R. A. *J. Comput. Chem.* **2007**, *28*, 1965–1973.
(112) Schnupf, U.; Willett, J. L.; Momany, F. A. *J. Comput. Chem.* **2010**, *31*, 2087–2097.
(113) Lopez, C. A.; Rzepiela, A. J.; de Vries, A.; Dijkhuizen, L.; Hunenberger, P. H.; Marrink, S. J. *J. Chem. Theory Comput.* **2009**, *5*, 3195.
(114) Bizzarri, A. R.; Cannistraro, S. *Phys. Rev. E* **1996**, *53*, R3040.
(115) Bagchi, B. *Chem. Rev.* **2005**, *105*, 3197–3219.
(116) Balasubramanian, S.; Bagchi, B. *J. Phys. Chem. B* **2001**, *105*, 12529.
(117) Sterpone, F.; Marchetti, G.; Pierleoni, C.; Marchi, M. *J. Phys. Chem. B* **2006**, *110*, 11504–11510.
(118) Faeder, J.; Ladanyi, B. M. *J. Phys. Chem. B* **2000**, *104*, 1033–1046.
(119) Tasaki, K. *J. Am. Chem. Soc.* **1996**, *118*, 8459–8469.
(120) Denisov, V. P.; Halle, B. *Faraday Discuss.* **1996**, *103*, 227–244.
(121) Magazù, S.; Migliardo, F.; Telling, M. *Eur. Biophys. J.* **2007**, *36*, 163–171.
(122) DeLano, W. L. *PyMOL*, version 1.1 ed.; Schrödinger, LLC: 2003.

JP109545V